Research Article | Vol. 26, No. 19 | 17 Sep 2018 | OPTICS EXPRESS 25399
Optics EXPRESS

Distributed acoustic sensor based on a two-mode fiber

MENGMENG CHEN,[1,2] ALI MASOUDI,[2,*] FRANCESCA PARMIGIANI,[2,3] AND GILBERTO BRAMBILLA[2]

[1]School of Electronics and Engineering, Nanjing Xiaozhuang University, Nanjing 211171, China
[2]Optoelectronics Research Centre, University of Southampton, Southampton, SO17 1BJ, UK
[3]Microsoft Research, Cambridge CB12FB, UK
[*]a.masoudi@soton.ac.uk

Abstract: A distributed optical fiber dynamic strain sensor also known as a distributed acoustic sensor (DAS) based on two-mode fiber is demonstrated. By using φ-OTDR interrogation technique, the backscattered light from higher order modes can be used to fully quantify vibrations along the sensing fiber. In addition, by combining the results obtained from different modes, 2.52dB improvement in noise floor is achieved. These results confirm that few-mode fibers can be used for DAS applications.

1. Introduction

In the past few years, few mode fibers (FMFs) have been adopted ever increasingly in communication systems as well as in areas such as high-voltage cable condition monitoring, pipeline leakage detection, fire detection, and environmental monitoring [1]. FMFs are used as a sensing medium in distributed optical fiber sensing due to their advantages such as higher nonlinear threshold level as well as higher capture fraction of the scattered light [2]. In FMFs, probe pulse with a higher energy can be used compared with that in single mode fibers (SMFs), resulting in a stronger backscattering which, consequently, leads to a better signal-to-noise ratio (SNR).

Several groups have started to study the advantages of Brillouin scattering in FMF, to develop new distributed optical fiber sensors (DOFS) for measurement of curvature [3], temperature [4, 5], and strain [6, 7]. For instance, in 2013, Li et al. demonstrated stimulated Brillouin scattering in propagating modes of a two-mode fiber using Brillouin optical time-domain analysis [8–10]. Weng et al. demonstrated a Brillouin optical time domain reflectometry (BOTDR) setup based on FMF and realized a DOFS capable of simultaneous temperature and strain measurement [11]. In another study, Wu et al. proposed a hybrid Raman and Brillouin optical time domain reflectometry system based on FMF to simultaneously measure the curvature and temperature distribution along the fiber. However, they have not taken advantage of the Brillouin or Raman scattering in each individual modes [12, 13].

In addition to Brillouin and Raman scattering, Rayleigh scattering in FMF has also been studied [2, 14]. In these studies, the authors have used the far field method to generalize the behavior of light scattering in multimode fibers [15]. They have numerically analyzed the capture fraction for different modes of a multimode step index fiber and for a range of different fiber parameters, including the core radius, the refractive index of the core and clad, and the numerical aperture (NA) and frequency of the launched radiation [2]. In addition, in 2016, Wang et al. established a general model for Rayleigh scattering in FMFs and verified the model experimentally [16].

In this study, a distributed acoustic sensor (DAS) based on two-mode fiber (2MF) and phase optical time domain reflectometry (φ-OTDR) interrogation technique is studied. A two-

#335513 https://doi.org/10.1364/OE.26.025399
Journal © 2018 Received 23 Jul 2018; revised 30 Aug 2018; accepted 2 Sep 2018; published 14 Sep 2018

Optics EXPRESS

mode step-index fiber is used as a sensing medium and the proposed sensing system takes advantage of the previously established sensing techniques developed by the authors [17, 18].

2. Principle

In order to analyze a DAS system based on a 2MF, the capture fraction and the mode coupling in FMF needs to be studied first.

In a FMF, the fraction of the power of the scattered light captured in a fixed mode (ν,μ) by an incident light propagating in the fundamental mode is given by [2, 14]:

$$B_{\nu\mu} = \frac{6q_{\nu}\Delta\pi^2}{V}\int_0^{\infty} F_{00}^2(\rho)F_{\nu\mu}^2(\rho)d\rho \tag{1}$$

where ν and μ are the indices of the mode. In this equation q_{ν} is introduced to differentiate radial and azimuthal modes. It acquires the unity value for azimuthal modes and 2 for radial modes. The value of Δ is given by $\Delta = (n_0^2 - n_1^2)/2n_0^2$, and n_0 and n_1 are the refractive indices of the core and cladding, respectively. V is the normalized frequency, $F_{00}(\rho)$ represents the field of the fundamental mode while $F_{\nu\mu}(\rho)$ is used to characterize the radial distribution of the mode (ν,μ).

Based on Eq. (1), if a signal is launched into the fundamental mode of a FMF, the scattered light couples into all the allowed modes in the fiber. If the intensity of the Rayleigh backscattered light for the LP_{01} mode is normalized to 1, the fraction of the intensity of the Rayleigh light backscattered in the LP_{11} mode would be 0.689 [2]. This equation is valid for any step-index FMF.

According to the analysis of reference [16], the total inter-mode crosstalk between the light propagating in the fundamental mode and in the LP_{11} mode would be –29.49dB, and the Rayleigh backscattered power is 37dB smaller than the injected power. Therefore, for the Rayleigh backscattering signal, the total inter-mode crosstalk among different backscattered modes should be 66.49dB smaller than the peak power of the probe pulse. Hence, it can be concluded that the phase of the Rayleigh backscattered light in one mode does not significantly affect that in other modes and the phase of different modes can be considered as independent.

So far, it is established that higher order modes support backscattered light and that the backscattered light in each mode propagates independently without significant cross-coupling. Therefore, it can be concluded that the backscattered light in different modes can be used for a DAS system. In this study, a 2MF is used for a φ-OTDR based DAS, and the performance of the newly designed φ-OTDR system is demonstrated. The basic principle governing the operation of the φ-OTDR based DAS is based on measuring the phase change between the coherent Rayleigh backscattering from two adjacent points of the sensing fiber. In this technique, a short pulse of light is launched into the fiber and the resultant backscattered coherent Rayleigh light is passed through an imbalanced Mach–Zehnder interferometer (IMZI) and onto a detector. The role of the IMZI is to mix the backscattered light from two adjacent points of sensing fiber in order to extract the phase-difference between them. The change in phase $\Delta\phi$ is directly proportional to the change in strain ε between the two points [18]:

$$\Delta\phi = 0.78\times\varepsilon\ell\beta \tag{2}$$

where ℓ is the distance between the two points and β is the propagation constant. The gauge length ℓ is equal to half the path difference between the two arms of the IMZI. This assumes that the pulse width is shorter compared to the length of the delay fiber. In this study, the phase demodulation method is similar to that of [19], and an IMZI with a symmetrical 3 × 3

Optics EXPRESS

coupler is used in the system to avoid phase signal fading [17]. The intensity at the three output ports is given by:

$$\begin{cases} I_1 = I_0[M + N\cos(\Delta\varnothing(t))], \\ I_2 = I_0[M + N\cos\left(\Delta\varnothing(t) + \frac{2\pi}{3}\right)], \\ I_3 = I_0\left[M + N\cos\left(\Delta\varnothing(t) - \frac{2\pi}{3}\right)\right]. \end{cases} \quad (3)$$

Using trigonometric identities and some mathematical manipulation, the phase change can be recovered as follows [19]:

$$\Delta\varnothing = \arctan\left(\frac{\overline{I_3} - \overline{I_2}}{\sqrt{3}\,\overline{I_1}}\right) \quad (4)$$

where $\overline{I_i}$ are the intensity of the light at the detectors less their DC components. A fringe-counting algorithm is implemented by looking at the transition of $\Delta\varnothing$ from + π/2 to -π/2 and vice versa [19].

3. Experimental setup

The experimental setup used in this study is shown in Fig. 1. A distributed feedback laser

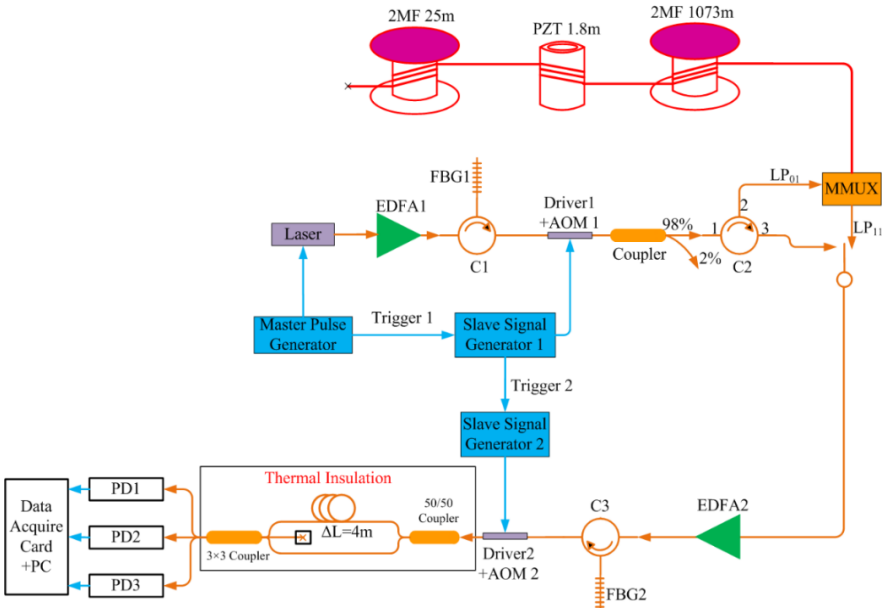

Fig. 1. Experimental setup based on 2MF. EDFA, erbium-doped fiber amplifier; AOM, acousto-optic modulator; C, circulator; FBG, fiber Bragg grating; PD, photodetector; MMUX: Mode Multiplexer.

diode with a wavelength of 1550nm was directly modulated to generate 18ns pulses with a repetition rate of 25μs. An erbium-doped fiber amplifier (EDFA1) was used to amplify the probe pulse to 5W peak power. The amplified pulses travel through a fiber Bragg-grating (FBG) filter (λ_0 = 1550.2nm; $\Delta\lambda$ = 0.4 nm; reflectivity = 99.9%) followed by the first acousto-

Optics EXPRESS

optic modulator (AOM1, insertion loss 3dB; extinction ratio = 50 dB). A FBG was used to remove the amplified spontaneous emission (ASE) from the EDFA1, while AOM1 was used to couple the amplified probe pulse to the sensing fiber. During the pulse-formation phase, AOM1 was turned on to allow the probe pulse to reach the sensing fiber, while during the signal detection stage, AOM1 was switched off to prevent the ASE from EDFA1 saturating the detectors . A 98/2 tap coupler was added to monitor the peak power and shape of the probe pulse. The probe pulse with a peak power of 2.5W was then launched into the mode multiplexer (MMUX) via the circulator C2.

The MMUX (CaiLAB) was used to selectively launch light into different modes of the 2MF. To test the response of the system to dynamic strains, 1.8 m of a 2MF fiber was wrapped around a ring piezoelectric transducer (PZT), 115 mm in diameter. A 1073 m and a 25 m long unstrained-unheated fiber were used before and after the PZT to separate the perturbed region from the sensing system and far end of the sensing fiber, respectively. The backscattered Rayleigh traces in the LP01 mode were collected by the third port of the circulator C2 while the backscattered traces in the LP_{11a} mode was collected from the corresponding LP_{11a} port of the MMUX. Both LP_{01} and LP_{11a} outputs were amplified by the second optical amplifier (EDFA2). The ASE from EDFA2 was filtered by FBG2 with similar parameters to FBG1.

During the pulse-formation period, AOM2 remained switched off to block the Fresnel reflection from MMUX saturating the detectors. When the Rayleigh backscattered light reached the front-end of the sensing fiber, AOM2 was switched on to allow the amplified backscattered light to pass through to the IMZI. The output of AOM2 was coupled into a thermally insulated IMZI with a path imbalance of 4 m using a 50/50 coupler. Three photodetectors (40 V/mA transimpedance; 125 MHz bandwidth) were used to detect the light from the 3 × 3 coupler at the output of the IMZI. The photodetectors were sampled using a 500 MHz bandwidth oscilloscope at a sampling rate of 1.25 GSa/s.

The refractive index (RI) of the sensing fiber was measured using an RI profiler (Fig. 2(a)). According to this profile, the sensing fiber had a step-index profile that supports two optical modes, LP_{01} and LP_{11}. Using COMSOL, the effective refractive indexes for LP_{01} and LP_{11a} modes at λ = 1550nm were calculated to be 1.4414 and 1.4392, respectively. The simulation results were obtained based on the extremely fine mesh size distribution of the fiber cross section in Fig. 2(b). The simulation results of the light field distributions for the two modes are shown in Fig. 2(c) and 2(d).

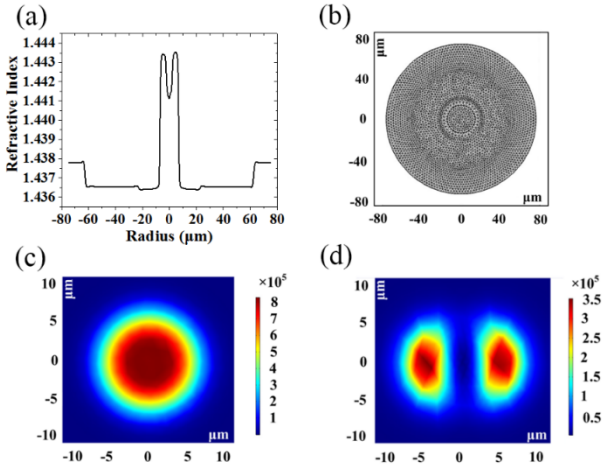

Fig. 2. Details of the two-mode fiber under test. (a) Refractive index profile, (b) Extremely fine mesh size distribution of distribution of the fiber cross section (c,d) Simulated mode field distribution of the LP01 and LP11 modes

Optics EXPRESS

4. Experimental results

Figure 3 present two time domain Rayleigh backscattered traces. The purple trace shows the backscattered light when the probe pulse is launched into the LP_{01} mode of the 2MF and the backscattering light is collected from the same mode. This will hereafter be referred to as LP_{01}-LP_{01} trace. The green trace, on the other hand shows the backscattered light when the probe pulse is launched into the LP_{01} mode while the backscattered light is collected from the LP_{11a} mode which, hereafter, will be referred to as LP_{01} - LP_{11} trace.

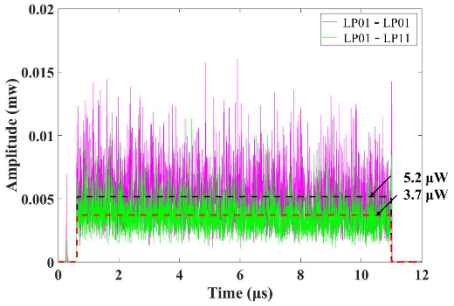

Fig. 3. Time-domain Rayleigh backscattered traces from the two different LP_{01} – LP_{01} and LP_{01} - LP_{11} cases.

Figure 4(a) shows the 3D diagram of the system for LP_{01}-LP_{01} trace in the time domain. A periodic oscillation can be observed at 1073m from the front end of the fiber with a minimum detectable strain of 20nε. Figure 4(b) shows the output of the sensing system in the spectral domain. The peak in the figure indicates a 1500Hz monotone vibration at 1073m with a peak strain level of 102.9nε. Similar results were obtained after the analysis of LP_{01}-LP_{11} trace.

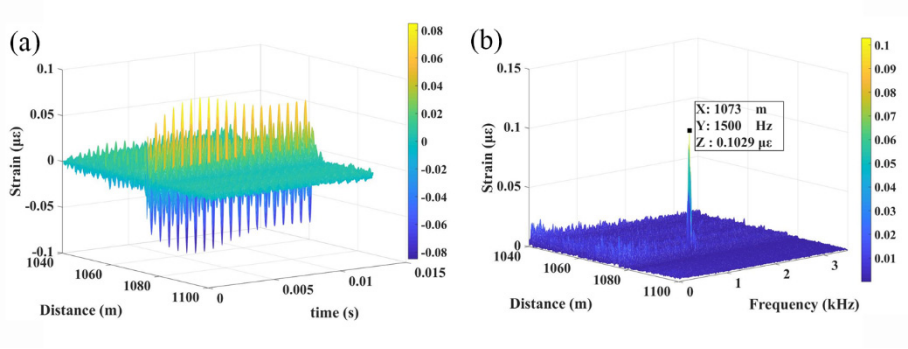

Fig. 4. (a) 3D plot of the phase-detector output in time domain for LP_{01} Mode. (b) 3D plot of the FFT of the phase-detector output for LP_{01} Mode.

To obtain the spectral and spatial profile for the section where an external perturbation was applied, two 2D cross-sections of the 3D diagram of Fig. 4(b) are provided in Fig. 5. Figure 5(a) shows the frequency spectrum of the dynamic fluctuations at a single point on the sensing fiber for both LP_{01}-LP_{01} (blue) and LP_{01}-LP_{11} (orange) traces. Figure 5(b) shows the spatial distribution of the strain along the sensing fiber at a fixed frequency. In this figure, the LP_{01}- LP_{01} trace is spatially shifted with respect to the LP_{01}- LP_{11} trace.

The strain response of the PZT as a function of the input voltage is shown in Fig. 6. Figure 6(a) shows the response to 1.5 kHz sinusoidal signal with voltages varying from $3V_{pp}$ to $18V_{pp}$. The orange circles represent the strain measured by the LP_{01}-LP_{01} traces while the blue circles represent that of LP_{01}-LP_{11} traces. The dashed lines in the two diagram show the voltage response of the PZT obtained using a conventional Mach-Zehnder Interferometer

Optics EXPRESS

(MZI). Figure 6(b) shows the average of the results from the LP_{01}-LP_{01} and LP_{01}-LP_{11} traces from Fig. 6 (a).

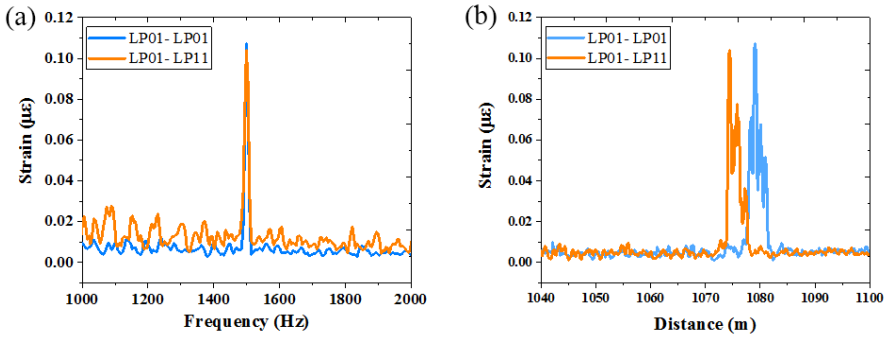

Fig. 5. 2D representation of the 3D diagram depicting the output of LP01 to LP01 and LP01 to LP11. (a) Frequency spectrum of the dynamic fluctuations at 1073m, showing a peak at 1500 Hz signal. (b) Spatial distribution of strain along the sensing fiber at 1500Hz.

Figure 7 demonstrates the frequency response of the sensor to different vibrational frequencies. The colored lines represent the data measured by the DAS system while the dashed line shows the PZT response measured by MZI. The data was collected by applying a fixed voltage ($8V_{pp}$) to the PZT while changing the frequency from 500 Hz to 3000 Hz. Figure 7(a) shows the sensor response to different vibrational frequencies using LP_{01}-LP_{01} traces while Fig. 7 (b) shows that of LP_{01}- LP_{11} traces.

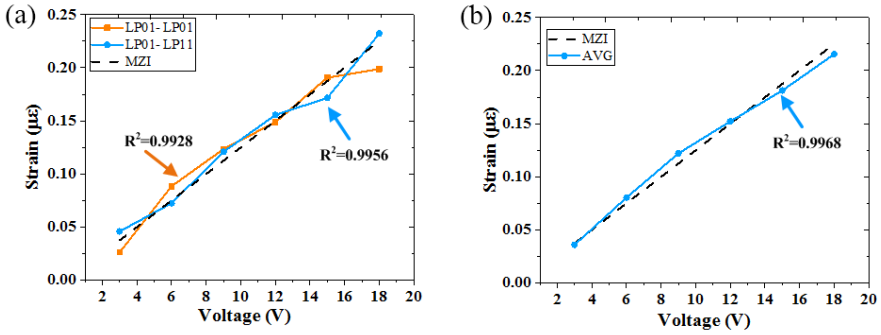

Fig. 6. Detected strain versus applied voltage for a 1.5 kHz sinusoidal signal. (a) LP_{01}- LP_{01} (orange line), LP_{01}-LP_{11} (blue line) and MZI (black dashed line); (b) averaged result (blue line) and MZI (black dashed line).

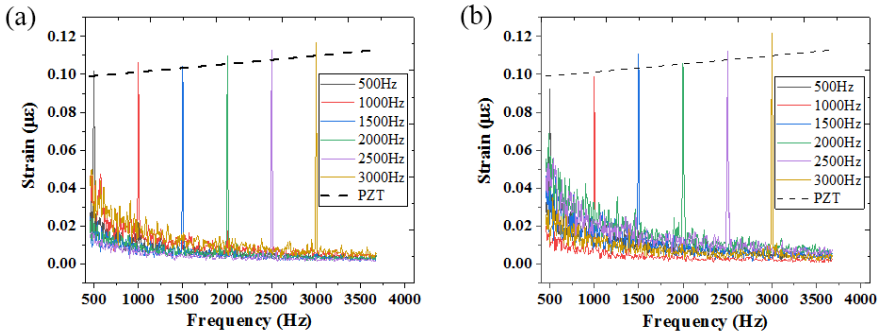

Fig. 7. Frequency response of the PZT measured by the distributed sensor and MZI (dashed line). (a) LP_{01}-LP_{01}, (b) LP_{01}-LP_{11}.

Optics EXPRESS

Similar results were obtain by launching light into the LP_{11a} mode and analyzing the backscattered light from both the LP_{01} and LP_{11a} modes.

Figure 8 shows the noise floor (NF) for the results obtain through analysis of LP_{01}-LP_{01} and LP_{01}-LP_{11} traces as well as the combined results from the two traces. The combined results showed 2.5dB improvement in the noise floor of the sensing system.

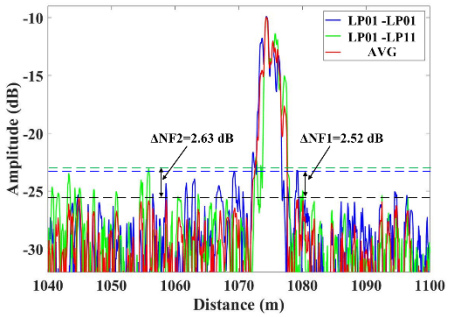

Fig. 8. Reduction of noise floor by combining the results from LP_{01}-LP_{01} and LP_{01}-LP_{11}.

5. Discussion

Figure 3 shows that the average Rayleigh backscattered powers are 5.2μW for the LP_{01} mode and 3.7μW for the LP_{11} mode after EDFA2. As the LP_{01}- LP_{01} traces travel from port2 to port3 of circulator C2, the attenuation between port2 and port3 (0.72dB) should be considered in the analysis of the backscattered Rayleigh power. In addition, the LP_{01}- LP_{01} traces encounter an additional loss of 0.27dB from the connectors. The 5.2μW backscattered power for the LP_{01}- LP_{01} traces is the total power of the Rayleigh backscattered light after considering the total loss 0.99dB. The ratio of the Rayleigh backscattering between LP_{01} and LP_{11} modes is 1: 0.711, which is in good agreement with the 1:0.689 ratio predicted in [2] through mathematical analysis.

The location of the sinusoidal perturbation on the 3D diagram of Fig. 4(a) matches the location at which the sensing fiber was attached to the PZT. Moreover, the frequency and amplitude of the oscillation agree with that of the input voltage to the PZT. This figure clearly shows the capability of the sensing system in localizing the position of the perturbation without any cross-talk between the perturbed and unperturbed region.

The peak in the 3D plot of Fig. 4(b) corresponds to the frequency and strain applied by the PZT at 1073m and demonstrates that the sensor can accurately measure the location, frequency, and strain of dynamic perturbations along the fiber.

Figure 5(a) shows the frequency spectrum of the perturbation at a single point on the 2MF. The minimum strain sensitivity of the results obtained through the analysis of LP_{01}-LP_{11} traces was measured to be 38nε which was slightly higher than that of the LP_{01}-LP_{01} traces with NF of 32nε. This can be associated with the lower intensity level of the LP_{01}-LP_{11} traces compared to LP_{01}-LP_{01} traces. The frequency and amplitude of both traces, however, demonstrate an accurate measurement of strain variation along the sensing fiber. The diagram of Fig. 5(b) represents the spatial distribution of strain along the sensing fiber. In this figure, the strain distributions for the LP_{01}-LP_{01} and LP_{01}-LP_{11} traces along the fiber are at different positions. This is due to the difference in the path length and group velocity between LP_{01}-LP_{01} and LP_{01}-LP_{11} traces. According to Fig. 1, LP_{01} - LP_{01} backscattered traces are transmitted through the circulator C2. Therefore, the length of the fiber attached to port 2 and 3 of the circulator (4.4m) should be included in the round trip time of the LP_{01} - LP_{01} traces. The LP_{01} - LP_{11} traces, on the other hand, directly couple to the EDFA2. Therefore, there is a 4.4m path difference in the strain distribution traces. Another factor influencing the perturbation location is the effective refractive indexes of the LP_{01} and LP_{11} modes. For

Optics EXPRESS

1100m long 2MF used in this experiment, the difference in the effective refractive indexes corresponds to 4.1ns temporal shift between the backscattered light in LP_{01} and LP_{11} modes.

Figure 6 shows a linear relationship between the amplitude of the input voltage to the PZT and the measured strain for a 1.5 kHz sinusoidal signal. The experimental results in Fig. 6 show that the proposed system is capable of reconstructing the strain with a linearity of R^2 = 0.9928 for LP_{01} - LP_{01}, R^2 = 0.9956 for LP_{01} - LP_{11}. By combining the results obtained from the analysis of the backscattered light from two modes, the linearity of the system was improved to R^2 = 0.9968 as shown in Fig. 6(b). The strain sensitivity of the sensor can be further improved through combining the data from higher order modes or by carrying out more measurements. Figures 6 and 7 show a good correlation between the data collected by the sensing system and the PZT response measured by the MZI.

The NF of Fig. 7(a) indicates a minimum detectable strain of 40nε for LP_{01} - LP_{01} traces at 500Hz while Fig. 7(b) shows a minimum strain sensitivity of 50nε for LP_{01} – LP_{11} traces. This can be associated to the higher SNR of LP_{01} - LP_{01} traces compared with that of LP_{01} – LP_{11} traces as shown in Fig. 3. The results obtain from the backscattered light in different modes can be combined to increase the SNR of the system. This improvement can be observed in Fig. 8 where the combined results of LP_{01} - LP_{01} and LP_{01} - LP_{11} traces have led to 2.5dB improvement in the noise floor. This improvement means that the sensitivity or range of the system can be improved by combining the backscattered light from different modes. It should be pointed out that the 1.1km sensing range used in this study was limited by our access to a longer length two-mode optical fiber.

These results prove that DAS systems [20–26] are capable of quantifying the frequency, strain, and location of dynamic perturbations anywhere along a FMF if the backscattered light from different modes are separated and analyzed individually by φ-OTDR technique. This shows that DAS systems can be modified to interrogate FMF installed in any infrastructure without the need to install new sensing fibers to monitor dynamic strains.

All the experimental results in this study were obtained by the data acquired from a single measurement and without averaging.

6. Conclusion

A distributed dynamic strain sensor using a two-mode sensing fiber is proposed and demonstrated. Since the scattered light is coupled from the fundamental mode into the higher order modes during the probe pulse propagates in a 2MF, φ-OTDR traces of both the LP_{01} and the LP_{11} modes can be used for dynamic strain analysis. 2MF based φ-OTDR demonstrated a sensing distance of 1100m and a spatial resolution of 2m. Such a system has the potential of improving the SNR by combining the phase from more FMF modes.

Funding

University Natural Science Research Project of Jiangsu Province (16KJB510019); High-Level Training Fund project of Nanjing Xiaozhuang University (2016NXY011); Engineering and Physical Sciences Research Council (EPSRC) - (EP/N00437X/1); and Zepler Institute Stimulus fund.

References

1. R. Singh, “Distributed Temperature Sensing (DTS) Market - Global Forecast to 2022,” Markets and Markets, 328799 (2016).
2. M. A. Bisyarin, O. I. Kotov, A. H. Hartog, L. B. Liokumovich, and N. A. Ushakov, “Rayleigh backscattering from the fundamental mode in step-index multimode optical fibers,” Appl. Opt. **56**(2), 354–364 (2017).
3. J. Chen, P. Lu, D. Liu, J. Zhang, S. Wang, and D. Chen, “Optical fiber curvature sensor based on few mode fiber,” Optik (Stuttg.) **125**(17), 4776–4778 (2014).
4. T. Huang, X. Shao, Z. Wu, Y. Sun, J. Zhang, H. Lam, J. Hu, and P. Shum, “A sensitivity enhanced temperature sensor based on highly Germania-doped few-mode fiber,” Opt. Commun. **324**, 53–57 (2014).

Optics EXPRESS

5. Q. Li, C. Lin, P. Tseng, and H. Lee, "Demonstration of high extinction ratio modal interference in a two-mode fiber and its applications for all-fiber comb filter and high-temperature sensor," Opt. Commun. **250**(4-6), 280–285 (2005).
6. A. Li, Y. Wang, J. Fang, M. J. Li, B. Y. Kim, and W. Shieh, "Few-mode fiber multi-parameter sensor with distributed temperature and strain discrimination," Opt. Lett. **40**(7), 1488–1491 (2015).
7. A. Kumar, N. Goel, and R. Varshney, "Studies on a Few-Mode Fiber-Optic Strain Sensor Based on LP01-LP02 Mode Interference," J. Lightwave Technol. **19**(3), 358–362 (2001).
8. A. Li, Q. Hu, and W. Shieh, "Characterization of stimulated Brillouin scattering in a circular-core two-mode fiber using optical time-domain analysis," Opt. Express **21**(26), 31894–31906 (2013).
9. A. Li, Y. Wang, Q. Hu, D. Che, X. Chen, and W. Shieh, "Measurement of distributed mode coupling in a few-mode fiber using a reconfigurable Brillouin OTDR," Opt. Lett. **39**(22), 6418–6421 (2014).
10. A. Li, Y. Wang, Q. Hu, and W. Shieh, "Few-mode fiber based optical sensors," Opt. Express **23**(2), 1139–1150 (2015).
11. Y. Weng, E. Ip, Z. Pan, and T. Wang, "Single-end simultaneous temperature and strain sensing techniques based on Brillouin optical time domain reflectometry in few-mode fibers," Opt. Express **23**(7), 9024–9039 (2015).
12. H. Wu, R. Wang, D. Liu, S. Fu, C. Zhao, H. Wei, W. Tong, P. P. Shum, and M. Tang, "Few-mode fiber based distributed curvature sensor through quasi-single-mode Brillouin frequency shift," Opt. Lett. **41**(7), 1514–1517 (2016).
13. H. Wu, M. Tang, M. Wang, C. Zhao, Z. Zhao, R. Wang, R. Liao, S. Fu, C. Yang, W. Tong, P. P. Shum, and D. Liu, "Few-mode optical fiber based simultaneously distributed curvature and temperature sensing," Opt. Express **25**(11), 12722–12732 (2017).
14. M. A. Bisyarin, O. I. Kotov, A. H. Hartog, L. B. Liokumovich, and N. A. Ushakov, "Rayleigh backscattering from the fundamental mode in multimode optical fibers," Appl. Opt. **55**(19), 5041–5051 (2016).
15. H. Hartog and M. P. Gold, "On the theory of backscattering in single-mode optical fibers," J. Lightwave Technol. **2**(2), 76–82 (1984).
16. Z. Wang, H. Wu, X. Hu, N. Zhao, Q. Mo, and G. Li, "Rayleigh scattering in few-mode optical fibers," Sci. Rep. **6**(1), 35844 (2016).
17. A. Masoudi, M. Belal, and T. P. Newson, "A distributed optical fibre dynamic strain sensor based on phase-OTDR," Meas. Sci. Technol. **24**(8), 085204 (2013).
18. A. Masoudi and T. P. Newson, "Analysis of distributed optical fibre acoustic sensors through numerical modelling," Opt. Express **25**(25), 32021–32040 (2017).
19. A. Masoudi and T. P. Newson, "High spatial resolution distributed optical fiber dynamic strain sensor with enhanced frequency and strain resolution," Opt. Lett. **42**(2), 290–293 (2017).
20. S. Liehr, Y. S. Muanenda, S. Münzenberger, and K. Krebber, "Relative change measurement of physical quantities using dual-wavelength coherent OTDR," Opt. Express **25**(2), 720–729 (2017).
21. Y. Muanenda, S. Faralli, C. J. Oton, and F. Di Pasquale, "Dynamic phase extraction in a modulated double-pulse ϕ-OTDR sensor using a stable homodyne demodulation in direct detection," Opt. Express **26**(2), 687–701 (2018).
22. A. Masoudi and T. P. Newson, "Contributed Review: Distributed optical fibre dynamic strain sensing," Rev. Sci. Instrum. **87**(1), 011501 (2016).
23. Y. Muanenda, "Recent Advances in Distributed Acoustic Sensing Based on Phase-Sensitive Optical Time Domain Reflectometry," J. Sens. **2018**, 3897873 (2018).
24. D. Davies, A. H. Hartog, and K. Kader, "Distributed vibration sensing system using multimode fiber," U.S. Patent No. 7 668 411 B2, 23 Feb. (2010).
25. A. E. Alekseev, V. S. Vdovenko, B. G. Gorshkov, V. T. Potapov, and D. E. Simikin, "Fading reduction in a phase optical time-domain reflectometer with multimode sensitive fiber," Laser Phys. **26**(9), 095101 (2016).
26. X. He, S. Xie, F. Liu, S. Cao, L. Gu, X. Zheng, and M. Zhang, "Multi-event waveform-retrieved distributed optical fiber acoustic sensor using dual-pulse heterodyne phase-sensitive OTDR," Opt. Lett. **42**(3), 442–445 (2017).